JOURNAL OF THEORETICAL AND APPLIED MECHANICS
61, 3, pp. 573-583, Warsaw 2023
https://doi.org/10.15632/jtam-pl/166461

DETERMINATION OF CONTACT PRESSURE DISTRIBUTION ON FRICTIONLESS ROUGH SURFACES USING AN OPTIMISATION APPROACH: A ONE-DIMENSIONAL STUDY

Milagros Noemi Quintana Castillo
Department of Mathematics, State University of Santa Catarina, Joinville, Brazil
e-mail: milla.quicas@gmail.com

Marco Antonio Luersen
Department of Mechanical Engineering, Federal University of Technology – Parana, Curitiba, Brazil
e-mail: luersen@utfpr.edu.br (corresponding author)

Francisco José Profito
Department of Mechanical Engineering, Polytechnic School of the University of São Paulo, Brazil
e-mail: fprofito@usp.br

Determining pressures and stresses that arise when mechanical components come into contact is crucial for analysis of surface-related failures. In real situations, determining contact pressure and stress distributions is challenging and depends on several factors, such as load, material properties and surface characteristics. This paper describes the determination of contact pressure on rough surfaces using a one-dimensional approach. Elastic, frictionless, unilateral, normal contact between a rough surface and a smooth surface is considered. Linear elastic half-space theory is used, and the contact pressure distribution is obtained by solving an associated optimisation problem. Results are given for a virtual wavy profile and two engineering roughness profiles.

Keywords: frictionless normal contact, rough surface, optimisation

1. Introduction

Contact problems in engineering have been studied for decades, particularly those related to elastic contact between deformable bodies. Research in this field is of considerable importance in mechanics since contact occurs between all interacting bodies that transmit forces and motion. When two bodies are pressed against each other, a contact area is formed in the interface between them, and a challenge is to determine the interfacial pressure and stress distributions developed in the vicinity of the contact zone (Zhao *et al.*, 2014). Jackson and Green (2006) and He *et al.* (2021) noted that stress analysis in materials in contact is of significant importance for design of mechanical components. According to Persson (2006), the study of contact between surfaces is also essential due to its influence on heat transfer, wear, friction and adhesion phenomena that significantly affect efficiency and durability of engineering systems.

All natural or manufactured surfaces are rough at the microscopic level and exhibit asperities at various length scale regardless of how they have been produced and even if they appear smooth macroscopically (Rey and Bleyer, 2018). The surface roughness also affects contact characteristics with a significant impact on the interfacial pressure and stress distributions and, consequently, on friction, wear and superficial damage behaviour (Jackson and Green, 2006). Therefore, it is essential to understand the nature of roughness and its effect on contact problems to analyse situations that correspond more closely to real applications (Weber *et al.*, 2018). According to Josso *et al.* (2002), surface topographies can be described as a superposition of

three components: form, waviness, and roughness. The contact mechanics between rough surfaces aims at explaining the complex interactions between asperities of the roughness component. Understanding the nature of these interactions is of great practical interest as they play a vital role in the tribological performance of different systems. However, understanding the relationship between the contact variables – such as interfacial pressure, stresses, real contact area, contact stiffness and many other aspects depending on morphological properties of the surfaces – remains challenging (Hills *et al.*, 1993; Bemporad and Paggi, 2015; Zhang *et al.*, 2019; Fu *et al.*, 2020).

In order to calculate the contact pressure distribution, the present work uses theory of elastic half-spaces to describe the normal frictionless contact problem between two bodies. Then, the contact regions of the bodies are discretised, resulting in a linear complementarity problem (LCP), which is converted into an optimisation problem and solved with a classic optimiser algorithm. Recently, LCPs have been used to solve optimisation problems, and in the last 20 years, elastoplastic analysis problems have also been solved by converting them into LCPs, which have emerged as a unified solution for quadratic and linear programming. According to Cottle *et al.* (1992) and Sushun (1995), the complementarity and linearity of an LCP provide necessary fundamental elements for the analysis and understanding of the complex nature of mathematical programming and equilibrium problems.

The contribution of this paper is twofold. First, it presents contact pressure solutions of real roughness profiles, which are not extensively used in studies with rough surfaces that usually represent asperities by analytic functions. The paper also uses an approach based on solving an associated optimisation problem, performed numerically by quadratic programming, a method that has not been widely used in the study of normal contact problems.

2. Formulation of the contact problem

2.1. Mathematical modelling of the contact problem

Two smooth non-conforming isotropic elastic bodies are considered to be initially in contact at a single point P. After applying an external normal force, both bodies deform in the vicinity of P, as shown in Fig. 1. At the interface between the bodies, contact pressures arise. The math-

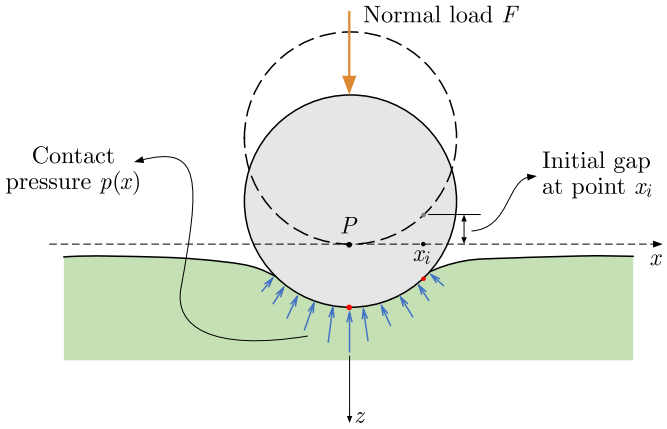

Fig. 1. Schematic representation of two smooth elastic bodies in contact

ematical formulation adopted in the present work to calculate the contact pressure distribution at the interface is based on the elastic half-space theory for normal frictionless line contact problems (Johnson, 1985; Zhao *et al.*, 2014). According to this theory, when two homogeneous linear elastic bodies with positive radii of curvature are brought into contact, and their deformations

are small enough for the theory of linear elasticity to be applicable, the dimensions of the corresponding contact area will be small compared with the radii of curvature of the undeformed surfaces. Since the region of interest is located in the vicinity of the contact area, the stresses can be calculated to a good approximation by considering each body as a semi-infinite elastic solid bounded by a flat surface, i.e., an elastic half-space. In addition, the following conditions for normal contact problems are considered: (i) there is no penetration between the two bodies, and thus the distance between the two surfaces is zero in the contact area and positive outside it; (ii) the pressure is zero outside the contact area. Mathematically

$$\begin{aligned} &e(x) = 0 \qquad p(x) \geqslant 0 \qquad \text{(points in the contact area)} \\ &e(x) > 0 \qquad p(x) = 0 \qquad \text{(points outside the contact area)} \end{aligned} \tag{2.1}$$

In the above equations, $p(x)$ is the interfacial pressure at the point x, $e(x) = u(x) + g(x)$ is the normal distance between the points on the surfaces after deformation, $g(x)$ is the initial gap between the surfaces before deformation, and $u(x)$ is the normal displacement at the point x. Considering elastic half-spaces, the normal displacement at the point x, induced by the pressure $p(x)$ distributed in the interval $I = [x_a, x_b]$ is given by Wang and Zhu (2020) as

$$u(x) = \frac{-4}{\pi E'} \int_{x_a}^{x_b} \ln|x - x'| p(x')\, dx' \tag{2.2}$$

where E' is the effective Young's modulus $E' = 2/[(1-\nu_1^2)/E_1 + (1-\nu_2^2)/E_2]$, E_1 and E_2 are Young's moduli, and ν_1 and ν_2 are Poisson's ratios of the materials of body 1 and body 2, respectively. The total normal force F is calculated as

$$F = \int_I p(x)\, dx \tag{2.3}$$

The solution of the contact problem should satisfy the contact conditions of Eqs. (2.1) and involves calculation of Eq. (2.2), which is generally obtained numerically by discretising the interval I with a uniform mesh and approximating the pressure profile by a piecewise constant function (see, for instance, Venner, 1991). Thus, the discretised form of Eq. (2.2) can be written as

$$u_i = u(x_i) = \sum_{j=1}^{j=N} K_{ij} p_j \qquad \text{or} \qquad \mathbf{u} = \mathbf{K}\mathbf{p} \tag{2.4}$$

where N is the number of discrete points and K_{ij} are the influence coefficients that compound the influence matrix $\mathbf{K}$, i.e.

$$\begin{aligned} K_{ij} = \frac{-4}{\pi E'} \int_{x_j - h/2}^{x_j + h/2} \ln|x_i - x'|\, dx' = \frac{-4}{\pi E'} \Big\{ &\Big|x_i - \Big(x_j + \frac{h}{2}\Big)\Big| \Big[\ln\Big|x_i - \Big(x_j + \frac{h}{2}\Big)\Big| - 1\Big] \\ - &\Big|x_i - \Big(x_j - \frac{h}{2}\Big)\Big| \Big[\ln\Big|x_i - \Big(x_j - \frac{h}{2}\Big)\Big| - 1\Big] \Big\} \end{aligned} \tag{2.5}$$

To solve the numerical problem, an N-dimensional vector $\mathbf{x} = [x_1, x_2, \ldots, x_N]$ is constructed with the coordinates of discrete points in the interval $I = [x_a, x_b]$. Likewise, the values of pressure $p(x)$, the gap between the surfaces before deformation $g(x)$, the normal displacement $u(x)$ and the gap between the surfaces after deformation $e(x)$ at each point x_i are also represented by the N-dimensional vectors $\mathbf{p}$, $\mathbf{g}$, $\mathbf{u}$ and $\mathbf{e}$, respectively.

In the present approach, the initial gap at the reference point g_0 must be provided. Therefore, the vector $\mathbf{g}$ containing the initial gap can be calculated based on the shapes (radii of curvature) of the contacting bodies as

$$\mathbf{g} = g_0\mathbf{1} + \mathbf{g}_s \tag{2.6}$$

where $\mathbf{g}_s$ is the normal distance between the contact surfaces defined from the reference point, and $\mathbf{1}$ is an N-dimensional unit vector. The normal force is obtained from Eq. (2.3) after the solution of $p(x)$ is found. Notice that for smooth surfaces, to have contact between the bodies, g_0 should be negative ($g_0 < 0$).

To account for the effect of surface roughness in the elastic half-space contact modelling approach, the function r describing the roughness heights is considered to define the initial gap. Accordingly, Eq. (2.6) can be rewritten as

$$\mathbf{g} = g_0\mathbf{1} + \mathbf{g}_s + \mathbf{r} \tag{2.7}$$

where $\mathbf{r}$ is the N-dimensional vector containing the roughness heights at the discrete points x_i.

Figure 2 depicts the initial undeformed contact geometry between a rough elastic flat surface (body 1 in Fig. 2) and a smooth rigid plane (body 2 in Fig. 2). It is important to remark that considering one of the surfaces smooth and rigid does not restrict the applicability of the current modelling approach, since two rough elastic surfaces can be transformed into the contact problem between a rough surface and a plane using equivalent parameters (Barber, 2018).

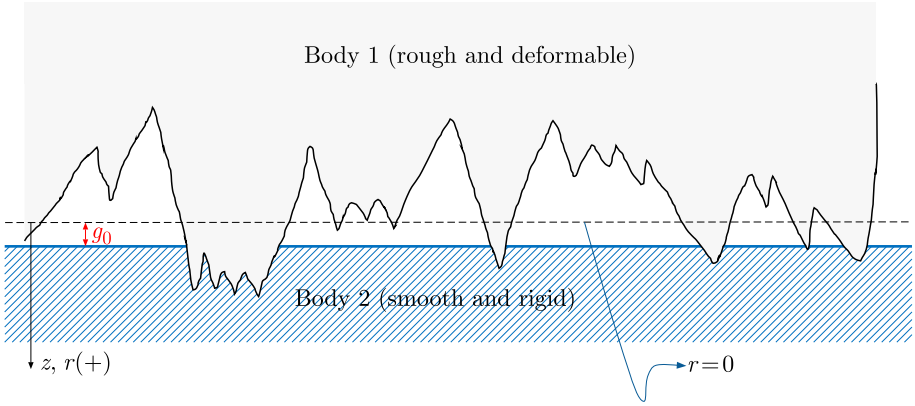

Fig. 2. Schematic representation of the initial undeformed contact gap between a rough flat elastic surface and a smooth rigid plane

2.2. Elastic normal contact problem as a linear complementarity problem

The contact conditions defined in Eqs. (2.1), and the distance between the contact surfaces after deformation can be written in discretised vector forms using Eq. (2.4) as

$$p_i e_i = 0 \rightarrow \mathbf{p}^{\mathrm{T}}\mathbf{e} = 0 \qquad \mathbf{e} = \mathbf{K}\mathbf{p} + \mathbf{g} \tag{2.8}$$

Therefore, to find the pressures at the discrete points, the following system of equations must be satisfied

$$\mathbf{e} = \mathbf{K}\mathbf{p} + \mathbf{g} \qquad \mathbf{p}^{\mathrm{T}}\mathbf{e} = 0 \qquad \mathbf{p}, \mathbf{e} \geqslant \mathbf{0} \tag{2.9}$$

The above equations can be identified as a linear complementarity problem (LCP). An important property of this LCP is that, as $\mathbf{K}$ is symmetric and positive definite, the solution is unique

(Bemporad and Paggi, 2015). The LCP described by Eq. (2.9) can be written as the following quadratic optimisation problem

$$\min_{\mathbf{p}} f(\mathbf{p}) \rightarrow \min_{\mathbf{p}}(\mathbf{p}^{\mathrm{T}}\mathbf{K}\mathbf{p} + \mathbf{p}^{\mathrm{T}}\mathbf{g})$$
$$\text{subject to: } \begin{cases} \mathbf{K}\mathbf{p} + \mathbf{g} \geqslant \mathbf{0} \\ \mathbf{p} \geqslant \mathbf{0} \end{cases} \tag{2.10}$$

The optimisation problem described in Eq. (2.10) is solved in Matlab using quadratic programming and an interior point algorithm presented in Byrd *et al.* (1999) and Nocedal and Wright (2006).

3. Numerical results and discussion

This Section discusses the numerical results obtained with the proposed calculation method for contact pressure of the three case studies. First, the profile of an analytical wavy surface is considered. Afterwards, the roughness profiles of two real engineering surfaces obtained from optical profilometry are analysed. For all cases, body 1 (the upper body) is assumed rough and body 2 (the lower one) smooth, following the formulation presented in Section 2.

3.1. Analytical wavy profile

This case evaluates the proposed calculation method for a wavy analytical profile. The geometric and material properties of the two contact bodies are shown in Table 1.

Table 1. Parameters for simulations of the analytical wavy profile

Body	Radius of curvature [mm]	Young's modulus [Pa]	Poisson's ratio [–]
1	20	$210 \cdot 10^9$	0.3
2	50	$210 \cdot 10^9$	0.3

The undulation of the wavy profile is chosen such that the peak heights are about 10 times smaller than the initial distance $g_0 = -0.01\,\mathrm{mm}$. Mathematically, this undulation is prescribed as

$$r(x) = 0.001\cos(50x) \qquad x \in [-1\,\mathrm{mm}, 1\,\mathrm{mm}] \tag{3.1}$$

To analyse the influence of the mesh discretization, simulations with meshes containing 64, 256 and 1024 nodes have been performed, and the results are summarised in Table 2. Figure 3 depicts the distance between the bodies in the initial condition. While the total force and contact width vary little as the number of nodes increases, the maximum pressure increases with the number of nodes. This increase can be explained by the highly accurate representation of the profile waviness as the mesh is refined, which yields a localized decrease in the real contact area and an increase in the local pressure.

Figures 4 show the pressure and gap distributions between the contact surfaces before and after contact for different meshes (64, 256 and 1024 nodes, respectively). The horizontal axis is normalised by a half-width of the Hertzian contact ($\overline{x} = x/b$). The contact pressure is normalised by its maximum value ($\overline{p} = p/p_{max}$) and is represented by the solid black line. The dotted blue and solid red lines represent the normalised initial ($\overline{g} = gR/b^2$) and final ($\overline{e} = eR/b^2$) gaps, respectively, where $R = 1/(R_1^{-1} + R_2^{-1})$ is the reduced radius of curvature, and R_1 and R_2 are the radii of curvature of body 1 and body 2.

Table 2. Simulation results of the analytical wavy profile.

No. of nodes	Normal force [N/mm]	Maximum pressure [MPa]	Contact width [mm]
64	856.7	2936	0.365
256	851.2	3991	0.341
1024	851.2	4036	0.333

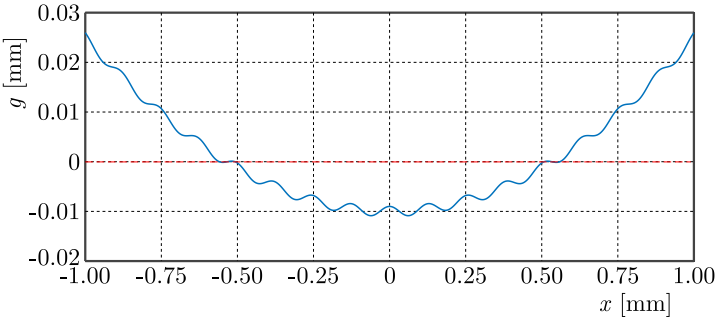

Fig. 3. Initial gap for the virtual wavy profile

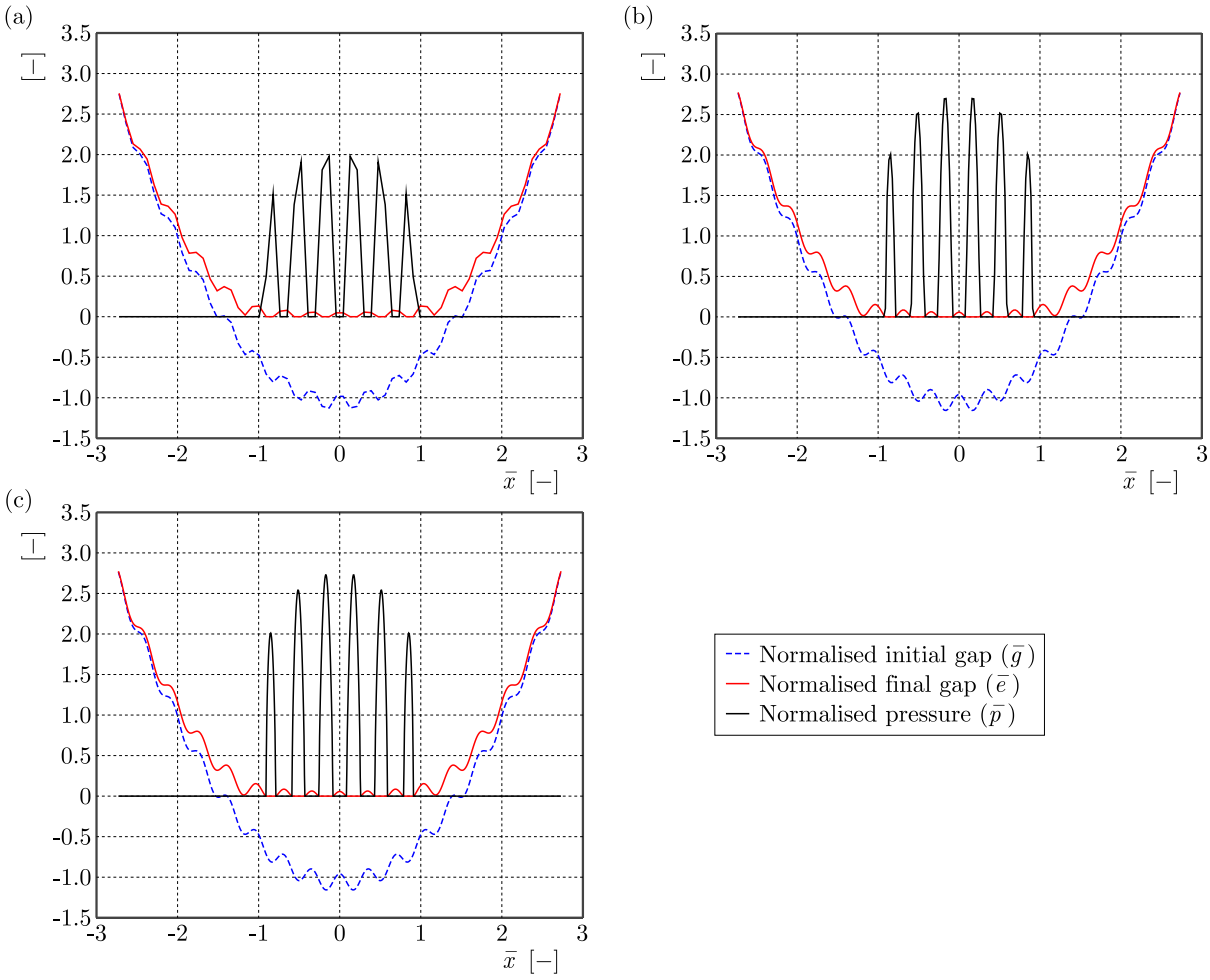

Fig. 4. Initial and final gaps and contact pressure for the analytical wavy profile. Results for meshes with (a) 64, (b) 256 and (c) 1024 nodes. All quantities are normalised

Overall, as can be observed in Fig. 4, wherever the pressure is nonzero and positive ($\overline{p} > 0$) the final gap is zero ($\overline{e} = 0$), and wherever the final gap is positive ($\overline{e} > 0$), the pressure is zero ($\overline{p} = 0$), thus satisfying the normal contact conditions of Eqs. (2.1). Figure 4 also shows the contact region between the normalised interval $\overline{x} \in [-1, 1]$. The pressure has a symmetrical distribution with six peaks, the largest being closer to the contact centre. Outside the contact region, as expected, the pressure is null. The pressure profile obtained with the 64-nodes mesh (Fig. 4a) is not smooth, and the maximum pressure is lower than those of the refined meshes. The pressure increases more smoothly with the 256-nodes mesh (Fig. 4b) but shows a flattening at the peaks. When the mesh discretization is increased to 1024 nodes (Fig. 4c), the entire pressure distribution becomes smooth, especially at the local maxima (peaks). In this latter case, the pressure peaks are also higher than those obtained with coarser meshes. This trend is because the greater the number of nodes, the more accurate the profile representation and solution near the peaks.

3.2. Real engineering surfaces

The cases presented below aim at evaluating the proposed calculation method for real engineering surfaces. To this end, a cylinder liner surface topography of an internal combustion engine and a 1200-grit sandpaper polished surface are considered. Both surfaces have been measured with 3D optical profilometry; the samples have 0.8×0.8 mm and 702×702 mesh points. The properties of the two surfaces are summarized in Table 3.

Table 3. Parameters for simulations of real engineering surfaces

Body	Radius of curvature [mm]	Young's modulus [Pa]	Poisson's ratio [–]
1	1000	$210 \cdot 10^9$	0.3
2	1000	$210 \cdot 10^9$	0.3

To perform 1D simulations, five profiles in the y-direction are considered. The initial distance g_0 is chosen to be approximately 0.2 times the standard deviation of the roughness heights. This value is defined following preliminary simulations and is intended to ensure that the real contact area is 4% to 10% of the apparent area. The real area is estimated by identifying and counting the regions of the discretized domain where the pressure is nonzero.

3.2.1. Surface of the cylinder of an internal combustion engine

Figure 5 shows, in three-dimensional and top views, the roughness profile obtained from measurements in a mesh of 702×702 points on a sample of the surface of the cylinder of an internal combustion engine.

In order to map the behaviour of the entire rough surface, analyses have been carried out in five cross-sections with discretization points corresponding to those used to measure the roughness profile (702 points). The sections were made parallel to the x axis, at positions $y = 0$; $y = 0.2$; $y = 0.4$; $y = 0.6$ and $y = 0.8$ mm. The initial reference gap value used was $g_0 = 9 \cdot 10^{-5}$ mm.

Table 4 shows, for different sections, the force and maximum pressure obtained in the simulations and height of the highest roughness peak in the section. The section where the highest contact force, 48 N/mm, occurs is the section with the highest roughness peak (section $y = 0.2$ mm), and sections that have the lowest force values (sections $y = 0.6$ and $y = 0.8$ mm) are also the sections where the highest roughness peaks are smaller than in the other sections. The same behaviour does not occur in the case of maximum pressure, i.e., there is no direct relationship

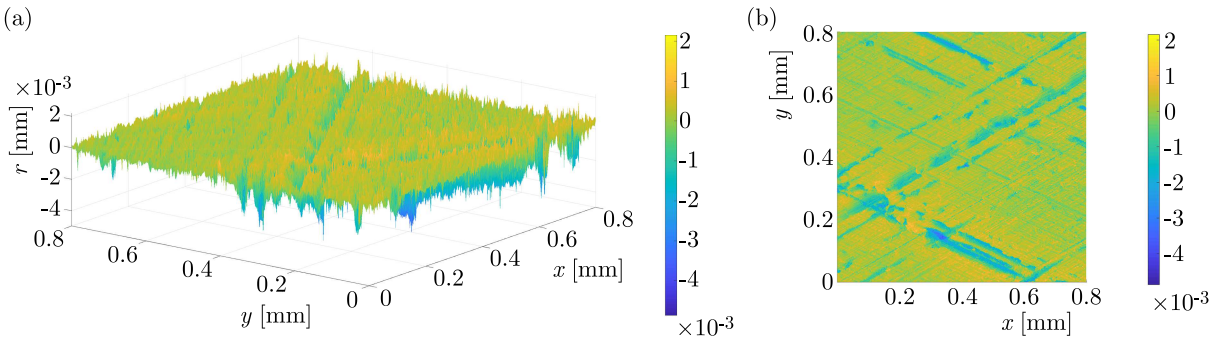

Fig. 5. Roughness profile of the surface of the cylinder of an internal combustion engine (702 × 702 mesh): (a) three-dimensional view, (b) top view – xy plane

Table 4. Results of simulations of the surface of the cylinder of an internal combustion engine

y [mm]	Force [N/mm]	Maximum pressure [MPa]	Highest roughness peak [mm]
0.0	35	6035	$7.0 \cdot 10^{-4}$
0.2	48	6480	$9.0 \cdot 10^{-4}$
0.4	32	8689	$7.2 \cdot 10^{-4}$
0.6	31	5181	$6.4 \cdot 10^{-4}$
0.8	31	5189	$6.4 \cdot 10^{-4}$

between the maximum pressure and the highest roughness peak, which occurs at $y = 0.4$ mm at the position $x = 0$.

Figure 6 shows, for the central section ($y = 0.4$ mm), the initial gap (dotted blue line) and the normal distance of each point on the surface after deformation (solid blue line) normalised by the maximum initial gap value[1]. The contact pressure (solid red line) normalised by its maximum

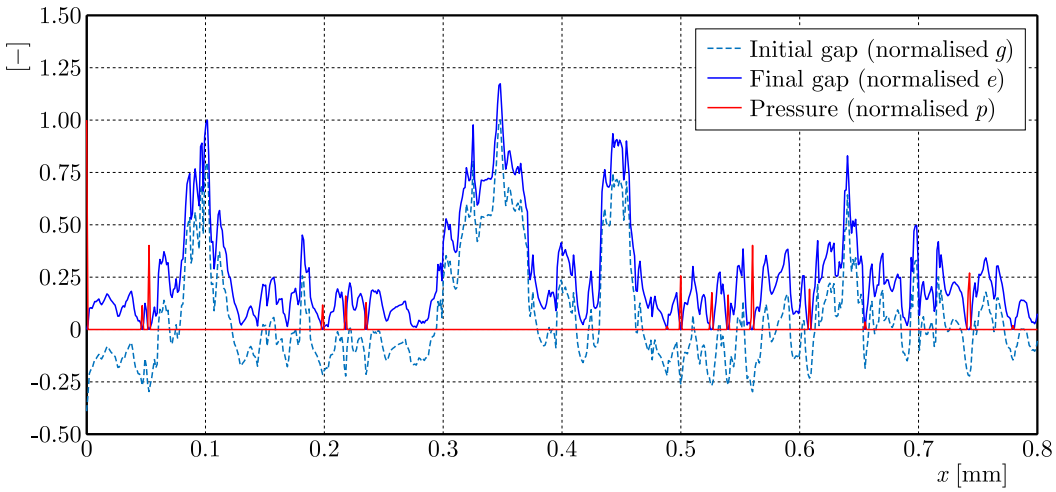

Fig. 6. Normalised initial and final gaps and normalised contact pressure for simulation of the surface of the cylinder of an internal combustion engine (section $y = 0.4$ mm)

value is also shown. From this figure, it can be noted that pressure occurs only where the final distance between the bodies is zero, i.e., where there is contact. Moreover, as expected, the final

[1]It is worth noting here that for this problem and the problem presented in Section 3.2.3 (i.e., for real engineering surfaces cases), the normalisation of the initial and final gaps (normalisations of g and e, respectively) are different from those used for the problem of Section 3.1. This is done aiming for clarity in presentation of the results.

shape of the piece undergoes changes. In addition, within a section, the point where the highest pressure occurs is the region with the highest roughness peaks, which corresponds to the highest initial "penetration", as can be seen when the initial gap (dotted blue line) and pressure (solid red line) are compared. For brevity, a graph of only a representative section is presented and discussed here and in Section 3.2.2.

3.2.2. Surface polished with 1200-grit sandpaper

Figure 7 presents, in three-dimensional and top views, the roughness profile obtained from measurements in a mesh of 702 × 702 points on a sample of a surface polished with a 1200-grit sandpaper. Because of the polishing, the roughness peaks are smaller compared with those of the surface of the cylinder of an internal combustion engine.

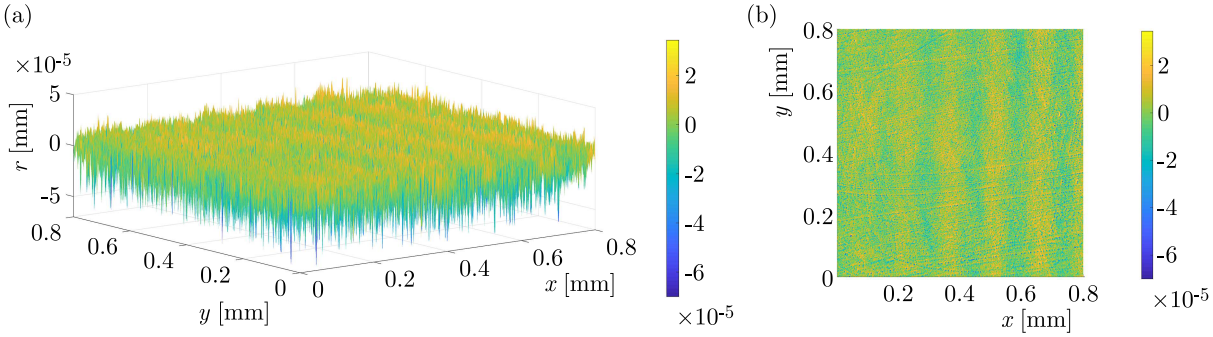

Fig. 7. Roughness profile of the surface polished with a 1200-grit sandpaper (702 × 702 mesh): (a) three-dimensional view, (b) top view – xy plane

As performed for the surface of the cylinder, simulations have been carried out in five sections. The initial reference gap value used was $g_0 = 1.4 \cdot 10^{-6}$ mm.

Table 5 presents, for different sections, the force and maximum pressure obtained from the simulations and the height of the highest roughness peak in the section.

Table 5. Results of simulations of the surface polished with a 1200-grit sandpaper

y [mm]	Force [N/mm]	Maximum pressure [MPa]	Highest roughness peak [mm]
0.0	1.11	309	$2.0 \cdot 10^{-5}$
0.2	1.04	153	$1.6 \cdot 10^{-5}$
0.4	1.20	203	$2.0 \cdot 10^{-5}$
0.6	1.11	310	$2.0 \cdot 10^{-5}$
0.8	0.86	114	$1.3 \cdot 10^{-6}$

Figure 8 shows, for the central section ($y = 0.4$ mm), the initial gap (dotted blue line) and the normal distance of each point on the surface after deformation (solid blue line) normalised by the maximum initial gap value. The contact pressure normalised by its maximum value is also shown (solid red line).

Because the surface has been polished, the roughness peaks have similar heights in all the sections, and there are only a few isolated peaks. This can also be observed in Table 5, where there are three sections, $y = 0$ mm, $y = 0.4$ mm and $y = 0.6$ mm: the highest peak measures $2.0 \cdot 10^{-5}$ mm, and two other sections have lower values, but still close ($1.3 \cdot 10^{-5}$ and $2.0 \cdot 10^{-5}$ mm). Thus, there is no significant variation in the contact force between the sections, and the highest value is at $y = 0.4$ mm. The highest maximum pressure occurs in the section with the highest

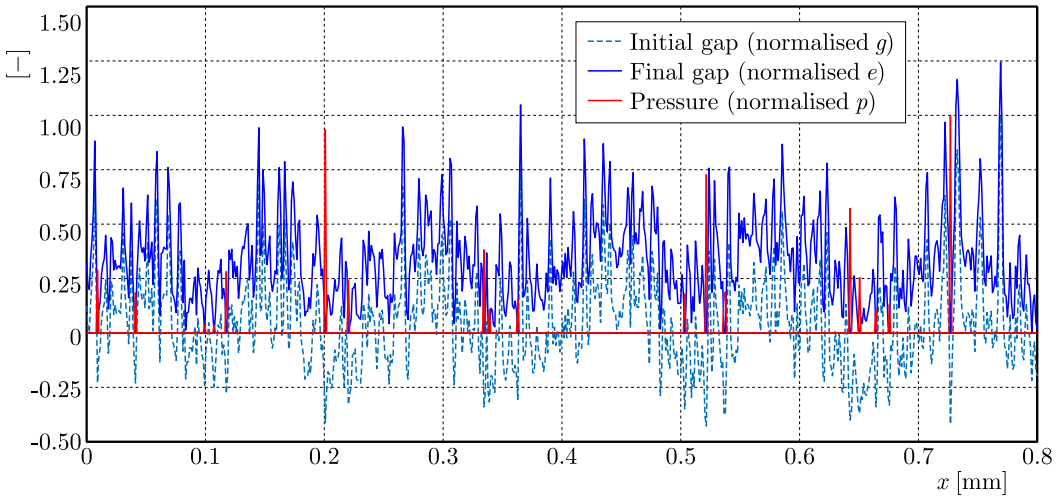

Fig. 8. Normalised initial and final gaps and normalised contact pressure for simulation of the surface polished with a 1200-grit sandpaper (section $y = 0.4\,\text{mm}$)

roughness peak ($y = 0.6\,\text{mm}$). As the heights of the peaks are more homogeneous than the peaks on the surface of the cylinder engine, the relationship between maximum the pressure and highest roughness peak is not so clear.

4. Concluding remarks

This work aims at developing and apply an efficient technique for determining contact pressure distribution between elastic bodies with rough surfaces. The corresponding problem is formulated as a linear complementarity problem (LCP), which is associated with an optimisation problem, and this is then solved using a quadratic programming strategy.

Problems with rough surfaces in a one-dimensional domain are analysed. Initially, a virtual surface is considered, i.e., with roughness generated by an analytic function, and then profiles of real engineering surfaces based on experimental roughness measurements are evaluated. Overall, the numerical results are coherent with what is observed in practice: the section where the highest contact force occurs is the one with the highest roughness peak, and the surfaces with higher roughness peaks have higher maximum pressures.

References

1. Barber J.R., 2018, Contact of rough surfaces, [In:] *Contact Mechanics. Solid Mechanics and its Applications*, Springer, **250**, 329-394

2. Bemporad A., Paggi M., 2015, Optimization algorithms for the solution of the frictionless normal contact between rough surfaces, *International Journal of Solid and Structures*, **69-70**, 94-105

3. Byrd R.H., Hribar M.E., Nocedal J., 1999, An interior point algorithm for large-scale non-linear programming, *SIAM Journal on Optimization*, **9**, 4, 877-900

4. Cottle R., Pang J., Stone R., 1992, *The Linear Complementarity Problem*, Philadelphia: Society for Industrial and Applied Mathematics

5. Fu S., Kor W.S., Cheng F., Seah L.K., 2020, In-situ measurement of surface roughness using chromatic confocal sensor, *Procedia CIRP*, **94**, 780-784

6. He X., Liu Z., Ripley L.B., Swensen V.L., Griffin-Wiesner I.J., Gulner B.R., Mcandrews G.R., Wieser R.J., Borovsky B.P., Wang Q.J., Kim S.H., 2021, Empirical relationship between interfacial shear stress and contact pressure in micro and macro-scale friction, *Tribology International*, **155**, 106780
7. Hills D.A., Nowell D., Sackfield A., 1993, *Mechanics of Elastics Contacts*, Butterworth-Heinemann
8. Jackson R.L., Green I., 2006, A statistical model of elasto-plastic asperity contact between rough surfaces, *Tribology International*, **39**, 9, 906-914
9. Johnson K.L., 1985, *Contact Mechanics*, Cambridge University Press
10. Josso B., Burton D.R., Lalor M.J., 2002, Frequency normalized wavelet transform for surface roughness analysis and characterization, *Wear*, **252**, 5-6, 491-500
11. Nocedal J., Wright S.J., 2006, *Numerical Optimization*, New York: Springer, 2a ed.
12. Persson B.N.J., 2006, Contact mechanics for randomly rough surfaces, *Surface Science Reports*, **61**, 4, 201-227
13. Rey V., Bleyer J., 2018, Stability analysis of rough surfaces in adhesive normal contact, *Computational Mechanics*, **62**, 1155-1167
14. Sushun K., 1995, The existence of the solution for linear complementary problem, *Applied Mathematics and Mechanics*, **16**, 7, 683-685
15. Venner C.H., 1991, Multilevel solution of the EHL line and point contact problems, PhD Thesis, University of Twente, Enschede, The Netherlands
16. Wang J., Zhu D., 2020, *Interfacial Mechanics: Theories and Methods for Contact and Lubrication*, New York: CRC Press, 1st ed.
17. Weber B., Suhina T., Junge T., Pastewka L., Brouwer A.M., Bonn D., 2018, Molecular probes reveal deviations from Amontons' law in multi-asperity frictional contacts, *Nature Communications*, **9**, 1, 888
18. Zhang F., Liu J., Ding X., Wang R., 2019, Experimental and finite element analyses of contact behaviors between non-transparent rough surfaces, *Journal of the Mechanics and Physics of Solids*, **126**, 87-100
19. Zhao J., Vollebregt E.A.H., Oosterlee W.C., 2014, A full multigrid method for linear complementarity problem arising from elastic normal contact problems, *Mathematical Modelling and Analysis*, **19**, 2, 216-240

Manuscript received March 20, 2022; accepted for print April 27, 2023